Nat. Hazards Earth Syst. Sci., 26, 6137–6155, 2026
https://doi.org/10.5194/nhess-26-6137-2026
© Author(s) 2026. This work is distributed under
the Creative Commons Attribution 4.0 License.

Natural Hazards and Earth System Sciences
Open Access
EGU

Detection of agricultural flash droughts using impact-informed thresholds

Ingrid Ubeda-Trujillo[1,2,3], **Micha Werner**[1,4], **Claudia Bertini**[1], **Miriam Coenders-Gerrits**[2], **and Graham Jewitt**[1,2]

[1]IHE Delft Institute for Water Education, P.O. Box 3015, 2601 DA Delft, the Netherlands
[2]Department Water Management, Delft University of Technology, P.O. Box 5048, 2600 GA Delft, the Netherlands
[3]Universidad Nacional Autónoma de Nicaragua, UNAN-Managua, Managua, Nicaragua
[4]Hydrology and Environmental Hydraulics Group, Wageningen University and Research, Wageningen, the Netherlands

Correspondence: Ingrid Ubeda-Trujillo (i.ubedatrujillo@tudelft.nl)

Received: 21 February 2026 – Discussion started: 10 March 2026
Revised: 5 November 2026 – Accepted: 8 November 2026 – Published: 25 November 2026

Abstract. Rapid and sustained evaporative stress can cause soils to lose moisture within days to weeks. When this rapid soil moisture depletion occurs during sensitive crop stages, it severely affects agricultural systems and manifests as agricultural flash droughts (AFDs). AFDs are often detected using fixed thresholds reported in the literature that assume uniformity across time and space, while rarely being linked to actual observed crop losses. However, this may poorly represent their occurrence and impacts in local contexts, thereby limiting their usefulness for decision-makers who require context-specific information. This study aims to overcome these limitations by introducing an impact-informed calibration of the Standardized Evaporative Stress Ratio (SESR) thresholds and linking them to observed crop losses. Thresholds are derived temporally across crop management periods and spatially across soil textures. The calibration is tested in the Central American Dry Corridor in Nicaragua, where rainfed agriculture predominates. Results suggest that evaporative stress signals differed between years with and years without drought-induced crop losses, with the clearest separation occurring during the crop-sensitive growing period in clayey soil textures. Results further show that, for these soils and during this period, calibrated thresholds provide a favourable balance between detecting years with drought-induced crop losses and reducing false alarms when compared with literature-based thresholds, whereas performance remains similarly low in sandy soils. Calibrated thresholds were considered skilful when they achieve high precision, high discrimination, and low uncertainty, and were identified during the pre-sowing and growing periods in moderately fine clay-loam and very fine expansive clayey soils. In loamy-silty soils, skilful thresholds were mainly observed during the pre-sowing period but not thereafter. Validation further shows that applying these skilful thresholds increases the detection of flash drought events associated with crop losses, with consistently higher hit rates than the literature-based thresholds. These findings indicate that monitoring AFDs using tailored, impact-informed thresholds has operational value for drought management and supports context-specific decision-making.

1 Introduction

One of the major climate-related hazards affecting crop yields, particularly in dryland regions dominated by rainfed systems, is drought (Kibler et al., 2023; Verbist et al., 2018). Drought arises when a prolonged lack of precipitation leads to low water availability in the soil, rivers, and reservoirs (Svoboda et al., 2002; Yuan et al., 2019). When these conditions are further intensified by high temperatures and evaporative stress that increase rapidly and persist over days to weeks, flash drought can develop (Basara et al., 2019; Noguera et al., 2022). Under these conditions, soils lose water faster than it is replenished, causing abrupt soil moisture decline and severely affecting agricultural systems (Yuan et al., 2019). When such rapid depletion affects the sensitive crop growth stages in rainfed systems (Verbist et al., 2018), the resulting conditions are commonly referred to as agricultural flash droughts (AFDs) (Lovino et al., 2024). These events often evolve over only a few weeks, leaving limited

time for farmers and institutions to adjust planting decisions, resource allocation, or short-term water management (Yuan et al., 2023). Because of the rapid onset and severe impacts on rainfed agriculture, AFDs are a critical climate-related risk that needs to be explicitly considered in early warning systems, risk management, and drought monitoring in dryland regions.

A widely used approach for flash drought detection relies on the Standardized Evaporative Stress Ratio (SESR), derived from the ratio of actual and potential evapotranspiration (Edris et al., 2023; Otkin et al., 2022). In most applications, flash droughts are detected using SESR with fixed percentile thresholds reported in the literature. These literature-based thresholds implicitly assume that a given percentile represents a comparable level of stress across regions and seasons. Yet percentiles are purely relative measures of rarity rather than of absolute stress, so a fixed percentile does not necessarily imply the same level of plant and soil-water stress everywhere (Hobbins and Huntington, 2016; Otkin et al., 2022). This assumption is particularly problematic in drylands with rainfed systems, because high evaporative demand and chronically low soil moisture make evaporative stress part of the normal background (Hobbins and Huntington, 2016; Kibler et al., 2023). In such settings, a fixed SESR percentile threshold does not consistently distinguish anomalous evaporative stress from background conditions across soil textures, and may not correspond to the same SESR levels at which agricultural impacts occur (Suliman et al., 2024; Yu et al., 2023). Furthermore, although SESR provides a signal of evaporative stress, it remains unclear under local dryland conditions whether this signal distinguishes years with drought-induced crop losses across soil textures from years without such losses. These issues highlight a broader methodological limitation of current SESR-based flash drought detection frameworks when applied across diverse climate and soil conditions.

Moreover, thresholds used in the literature are usually defined independently of crop growth stages, even though short dry spells during sensitive growth stages can cause damage (Verbist et al., 2018), while a similar stress outside these stages has limited impact (Bucheli et al., 2021; Teleubay et al., 2025). This creates a gap between when SESR anomalies are detected (Nguyen and Choi, 2024) and when impacts occur in the local context (Shyrokaya et al., 2024; Walker et al., 2024). While other indicators, such as the Vegetation Health Index (VHI), provide direct evidence of agricultural stress on the ground, they are reactive, signalling stress only after it has occurred (Li et al., 2023; Rojas, 2020). SESR, in contrast, responds earlier to anomalies in the surface energy and water balance (Anderson et al., 2016; Hobbins and Huntington, 2016), offering a timely physically based signal of evaporative stress that has the potential to support operational use (Buitink et al., 2021; Leasor et al., 2020; Li et al., 2023; Teleubay et al., 2025) when appropriately calibrated to observed crop losses (McEwen et al., 2021; Shyrokaya et al., 2024). This suggests that SESR could support detection and monitoring of agriculturally relevant flash drought conditions if thresholds were calibrated to local farming conditions and impact evidence. However, there is still no widely applied approach to systematically calibrating SESR thresholds across both crop management periods and soil textures, particularly in dryland, rainfed systems, which limits the operational relevance of SESR for agricultural flash drought monitoring and management.

In many dryland regions, the aforementioned limitations are particularly critical for smallholder rainfed systems, where flash droughts can quickly translate into crop failure, food insecurity, and income loss (Solh and van Ginkel, 2014; van der Zee Arias et al., 2012). This has occurred in the Central American Dry Corridor in Nicaragua, where recurrent drought episodes have been associated with declining crop yields and heightened vulnerability among smallholder farmers. Therefore, strengthening agricultural flash drought detection requires context-specific information that is essential for drought monitoring and management. This study addresses these limitations by calibrating SESR thresholds temporally across crop management periods and spatially across soil textures using a benchmark of agricultural impacts. Crop management periods refer to the pre-sowing (April), sowing (May), and growing (June–July; covering vegetative, flowering, and grain-filling stages of maize and beans) periods of the local crop calendar. To achieve this aim, the specific objectives of this study are to:

(i) determine whether evaporative stress signals represented by SESR discriminate between years with and years without drought-induced crop losses,

(ii) derive and evaluate skilful impact-informed SESR thresholds across crop management periods and soil textures, and

(iii) validate literature-based and calibrated impact-informed SESR thresholds against agricultural impact benchmarks.

In a wider context, this study enhances the agricultural relevance of SESR-based AFD detection by providing impact-informed thresholds across crop management periods and soil textures. This can provide farmers and decision-makers with more context-specific information in dryland rainfed systems, where crop losses can directly affect crop production and household income. In this sense, the study also supports progress towards Sustainable Development Goals 1 (No poverty), 2 (Zero hunger), and 13 (Climate action). Although the calibration was tested in the Dry Corridor of Nicaragua, this work provides a basis for adaptation and further testing in other dryland rainfed regions and for integrating locally informed, impact-based agricultural flash drought monitoring into drought management.

2 Methods

2.1 Overview of the study area: climate, agricultural, and edaphic context

To develop and test the calibration process, this study focuses on the Nicaragua Dry Corridor, specifically in the northern part of the Rio San Juan basin. This basin comprises eight hydrological catchments and includes major rivers such as the Sinecapa and Pacora (INETER et al., 2014). The basin spans diverse landscapes. The northern part overlaps with protected areas including Yalí, Miraflor-Moropotente and Tizey-Estanzuela. The middle part includes Lake Managua, several crater lagoons and additional protected areas, while the southernmost part comprises the Tisma wetland, a Ramsar site. In total, the basin encompasses 31 municipalities and approximately 640 settlements. At a broader scale, the study area forms part of the Central American Dry Corridor, which includes the countries of Guatemala, El Salvador, Honduras, and Costa Rica, bounded by the Caribbean region to the east and the Pacific Ocean to the west.

Figure 1a shows that rainfed agriculture covers approximately 40 % of the study area (Teluguntla et al., 2023; Ubeda Trujillo and Rocha, 2020) with subsistence and commercial farming based on the main staples: beans and maize (van der Zee Arias et al., 2012). The main cropping cycle extends from May to August, lasting about four months and including pre-sowing, sowing, growing (vegetative, flowering, and grain filling stages), and harvesting periods (Fig. 1c). This cropping cycle coincides with the rainy season (Fig. 1c). The average annual precipitation is about 800 mm yr^{-1} , and mean temperatures are above 25 °C for the whole year (van der Zee Arias et al., 2012). A notable climatological feature is the Canícula, a 10–20 d mid-summer dry spell, commonly occurring from mid-July to August linked to the El Niño-Southern Oscillation (Rojas et al., 2020). The Canícula temporally interrupts the rainy season and tends to intensify during El Niño years (Verbist et al., 2018). Atmospheric evaporative demand varies across climatic seasons and regions within the study area. During the dry season, in the east-central and south-central parts of the Pacific plains (46–80 m a.s.l.), mean daily potential evaporation (PET) reaches 8.5–9.3 mm d^{-1} based on the analysis of the MOD16A2 dataset by Salinas Marcenaro et al. (2023). In contrast, in the north-eastern and western parts of the mountainous areas (682–1004 m a.s.l.), PET ranges from 7.5–8.3 mm d^{-1} (Salinas Marcenaro et al., 2023), reflecting elevated atmospheric evaporative demand before the onset of rains. PET decreases in both regions during the rainy season, with values of 4.5–6.0 mm d^{-1} in the Pacific plains and 3.5–4.5 mm d^{-1} in the mountainous ranges (Salinas Marcenaro et al., 2023). Overall, the Pacific shows the highest evaporative demand throughout the year, while the northern mountain region exhibits the lowest PET, following a common annual pattern governed by the transition from the rainy to the dry season. The study area is characterised by six soil textures (DGOT–INETER, 2024): (1) coarse sandy, (2) moderately coarse sandy, (3) loamy and silty, (4) moderately fine clay-loam, (5) fine clayey, and (6) very fine expansive clayey soils (see Fig. 1b).

2.2 Data sources and preprocessing

2.2.1 Remote sensing and qualitative data preparation

Three main sources of data were used: (1) qualitative information such as newspapers and reports, (2) MODIS-derived actual and potential evapotranspiration (ET and PET; MYD16A2GF; Running et al., 2021), and (3) Vegetation Health Index (VHI; FAO, 2014). The MODIS MYD16A2GF dataset provides 8 d composite data at 500 m × 500 m spatial resolution. The dataset is available from 2001 onwards (Running et al., 2021). The Vegetation Health Index (VHI) dataset has a 1 km × 1 km spatial resolution and a decadal (10 d) temporal resolution. The dataset is available from 1984 onward (FAO, 2014).

Qualitative information related to years with drought-induced crop loss impacts was compiled from the two oldest national newspapers in Nicaragua and from reports produced by GIEWS (Global Information and Early Warning System on Food and Agriculture; https://www.fao.org/giews/reports/giews-updates/en/, last access: 27 January 2024), FEWS NET (Famine Early Warning Systems Network; https://fews.net/, last access: 27 January 2024), and EM-DAT (The International Disaster Database; https://www.emdat.be/, last access: 27 January 2024). Digital archives were systematically searched using drought- and impact-related keywords in Spanish and English, including "drought", "sequía", "lack of rain", "falta de lluvia", "lluvias tardan en llegar", "crop loss(es)", "pérdida de cosecha", "yield reduction", and combinations of these terms. For each candidate newspaper article or report, the information was organised into three levels of detail, each presented separately. The first level includes the publication date and a short description of the reported impacts for each source. The second level provides the impact timing, the type of impacts reported (e.g. economic, agricultural, population affected), and the sources. The third level summarises the impact year, the crop impacts, and the sources reporting those impacts.

From the MYD16A2GF dataset (Running et al., 2021), actual evapotranspiration (ET) and potential evapotranspiration (PET) input data from 2001–2024 were used to derive the Standardized Evaporative Stress Ratio (SESR) following the approach of Christian et al. (2019), as follows:

$$\mathrm{SESR}_{ijp} = \left(\mathrm{ESR}_{ijp} - \overline{\mathrm{ESR}}_{ijp}\right) / \sigma\mathrm{ESR}_{ijp} \quad (1)$$

where SESR_{ijp} is the z-score of ESR at grid point (ij) and time step p. ESR_{ijp} is the evaporative stress ratio calculated as ET/PET, $\overline{\mathrm{ESR}}_{ijp}$ is the mean ESR for a time step p, and $\sigma\mathrm{ESR}_{ijp}$ is the standard deviation of ESR across all years.

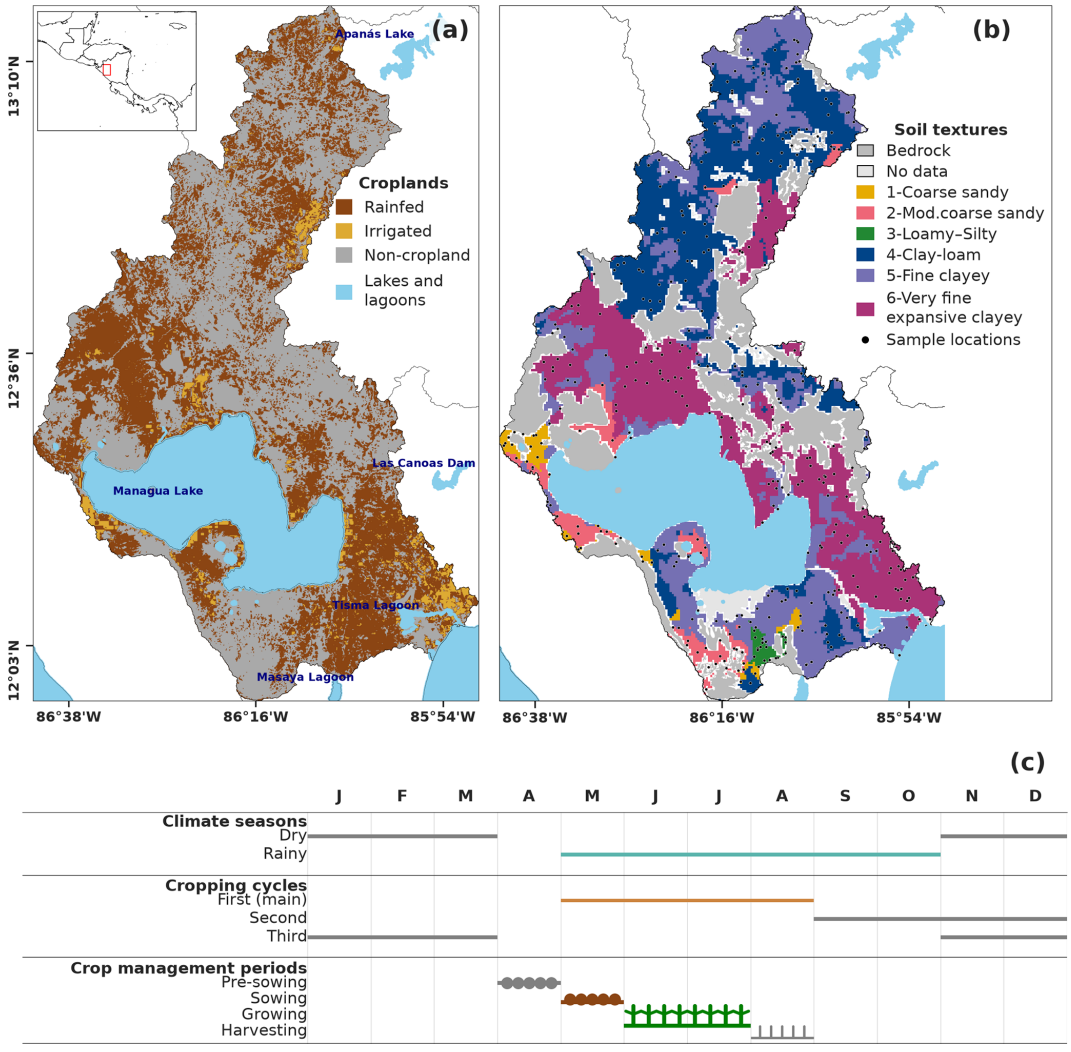


Figure 1. Overview of the northern part of the Rio San Juan basin. **(a)** croplands, **(b)** soil textures, **(c)** climate seasons and crop calendar (maize and bean growing period).

Temporal changes in SESR (ΔSESR) are calculated as:

$$(\Delta\mathrm{SESR}_{ijp})_z = \left(\Delta\mathrm{SESR}_{ijp} - \overline{\Delta\mathrm{SESR}}_{ijp}\right)/\sigma\,\Delta\mathrm{SESR}_{ijp} \quad (2)$$

Where $(\Delta\mathrm{SESR}_{ijp})_z$ is the standardised change of SESR at specific grid point (ij) and time step p. $\overline{\Delta\mathrm{SESR}}_{ijp}$ and $\sigma\,\Delta\mathrm{SESR}_{ijp}$ are the mean and standard deviation, respectively.

The VHI dataset (FAO, 2014) from 2000 to 2024 was used to identify drought-induced crop loss years and to validate and calibrate SESR thresholds. Seven preprocessing steps were applied to ensure quality and temporal/spatial compatibility with the MODIS-based SESR dataset. These included: filtering values outside the valid range 0–1 (Kogan, 1995); smoothing persistent saturation values (VHI = 1) (Gu et al., 2013); converting decadal labels to ISO 8601 dates; resampling VHI to 8 d intervals to align with the temporal resolution of the MODIS-based SESR product; filling temporal gaps with linear interpolation (Soltani et al., 2004); filling spatial voids using nearest-neighbour interpolation within valid data areas (Teoh et al., 2008); and comparing the original and resampled datasets at various spatial points to evaluate harmonisation reliability.

2.2.2 Sampling design

The period of analysis was from February to August from 2000–2024. February to April is considered an early warning opportunity window, since early evaporative stress signals during these months may condition soil moisture availability before the sowing period (May). Within this period, April is considered a critical pre-sowing month, as high evaporative stress during this month can reduce soil moisture availability for germination following sowing. Sowing typically occurs in May, with the main growing period of maize and beans in June–July, while August is the end of the main

cropping cycle. Across the study, a point-based sampling design was used as the common spatial basis for extracting and analysing the gridded datasets, rather than considering every 500 m grid point. The number of sample points was determined according to the spatial representation of each soil texture, while ensuring a minimum of 30 points per soil texture. This sampling design resulted in 388 points (Fig. 1b), with an average inter-point spacing of approximately 3 km. Data from the gridded products were extracted at these sample locations throughout the study. These sample points were retained for threshold calibration to reduce the computational burden while maintaining representation across soil textures.

2.3 Calibrating impact-informed SESR threshold

Christian et al. (2019) proposed SESR criteria for both drought onset and rapid intensification to identify flash droughts. This study replaces the fixed drought onset threshold defined in literature with a calibrated, impact-informed SESR threshold specific to crop management period and soil textures. The threshold criteria used by Christian et al. (2019) to detect rapid intensification, a condition in identifying flash droughts are retained. The spatial and temporal calibration of SESR thresholds is summarised in five parts, which are described in the sub-paragraphs below. First, the drought-induced agricultural impact benchmarks are described in Sect. 2.3.1. The conceptual approach to detect agricultural flash drought is then detailed in Sect. 2.3.2. In Sect. 2.3.3, differences in evaporative stress signals, represented by SESR are established between years with and years without drought-induced crop losses. Section 2.3.4 then presents the threshold optimisation, uncertainty estimation, and selection of skilful calibrated impact-informed SESR thresholds. Finally, the validation strategy against agricultural benchmarks is detailed in Sect 2.3.5.

2.3.1 Establishing drought-induced agricultural impact benchmarks

Two agricultural impact benchmarks related to drought-induced crop losses were developed; one based on the Vegetation Health Index (VHI) and a second derived from newspapers and reports. The VHI-based benchmark was used to identify impact-relevant years for calibration, whereas both benchmarks were used to validate literature-based and calibrated SESR thresholds. The benchmarks were obtained as follows:

VHI-based drought-induced crop losses benchmark: years with drought-induced crop losses were obtained from the Vegetation Health Index (FAO, 2014; Fig. 2). Crop losses were indicated when VHI values fall below 0.35 at the end of the first cropping cycle in August (Fuganti et al., 2020). Earlier-season VHI conditions were excluded from defining crop losses, as early-season vegetation stress does not necessarily translate into end-of-season crop losses (Fuganti et al., 2020). This benchmark of years with crop losses was constructed independently for each of the 388 sample locations before grouping the resulting time series by soil texture class. Figure 2 shows the years in which crop losses were identified using the VHI data as a marker in August. Note that the figure shows years with losses for one sample location and does not necessarily imply region-wide impacts.

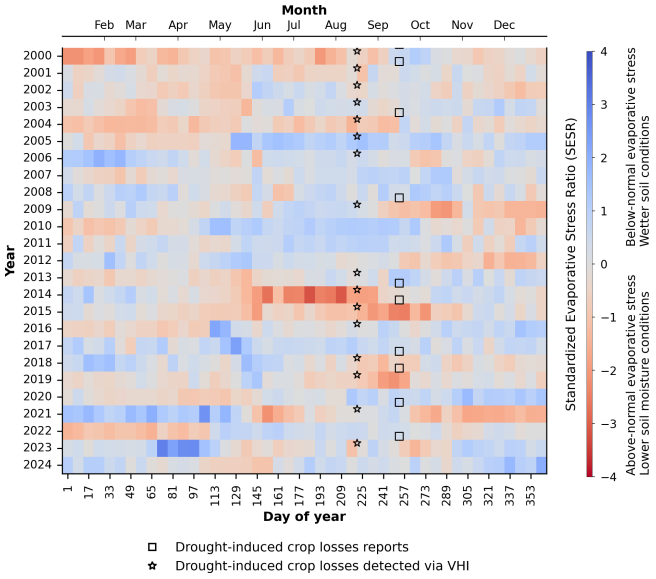


Figure 2. Years with crop losses derived from the Vegetation Health Index and reports at one representative sample location within the study area characterised by moderately fine clay-loam soil. The heatmap represents the median of the Standardized Evaporative Stress Ratio (SESR) across the sampled locations aggregated at each 8 d interval.

Reported drought-induced crop losses benchmark: using the two newspapers and reports from GIEWS, FEWS NET and EMDAT and organised as explained in Sect. 2.2.1, years with reported drought-induced crop losses were retained only when these were documented by at least three independent sources. To harmonise the timing of reported impacts, each reported event was reassigned to one-month window centred on September. As the reported impacts from the sources were found not to be consistent in the indication of location or spatial extent, the benchmark was interpreted as representative of drought-impact conditions across the broader region rather than specific to the soil texture scale.

2.3.2 Detecting agricultural flash droughts

In the Standardized Evaporative Stress Ratio (SESR) framework described by Christian et al. (2019) (hereafter referred to as the literature-based approach), a flash drought event must satisfy four criteria: (i) a minimum duration of 30 d; (ii) the final SESR value at the end of the rapid intensification period falls below the 20th percentile (P20) of the SESR distribution; (iii) ΔSESR between consecutive time steps must

be at or below the 40th percentile (P40) of the ΔSESR distribution. An exception is permitted between consecutive intervals, where ΔSESR may exceed P40, provided that in the following interval ΔSESR returns to ≤ P40 and the SESR falls below the value it had prior to the exception. And (iv) the mean ΔSESR during the entire event remains below the 25th percentile (P25) of the ΔSESR distribution. Criteria (i) and (ii) represent the drought component of flash drought, whereas criteria (iii) and (iv) characterise its rapid intensification. These thresholds have also been applied in other studies (cf. Gou et al., 2022; Nguyen and Choi, 2024). In this study, the fixed 20th percentile drought criterion is replaced by a calibrated SESR threshold $\Theta_{t,k}$ specific to crop management period t and soil texture classes k using an agricultural drought-impact benchmark. An agricultural flash drought (AFD) was identified only when SESR remained below the calibrated threshold while the ΔSESR rapid-intensification criteria were simultaneously satisfied for at least four consecutive 8 d intervals (32 d). The rapid intensification criteria of Christian et al. (2019) were retained unchanged. Accordingly, an AFD was defined as:

$$\mathrm{AFD}_{t,k} = \begin{cases} 1, \text{ if } \mathrm{SESR}_{p,t,k} \le \Theta_{t,k} \wedge \Delta\mathrm{SESR}_{p,t,k} \le \mathrm{P40} \\ (1 \text{ exeption allowed}) \wedge \overline{\Delta\mathrm{SESR}}_{s,t,k} \le \mathrm{P25} \\ 0, \text{ Otherwise} \end{cases} \quad (3)$$

where $\mathrm{AFD}_{t,k}$ denotes the presence (1) or absence (0) of an agricultural flash drought. $\mathrm{SESR}_{p,t,k}$ is the Standardized Evaporative Stress Ratio at 8 d interval (p) within crop management period (t), for a sample falling within a soil texture class (k). $\Theta_{t,k}$ is the SESR threshold to be calibrated specific to crop management period (t) and the soil texture class associated with sample (k), which is applied to each 8 d interval (p) within the corresponding crop management period and soil texture class. $\Delta\mathrm{SESR}_{p,t,k}$ is the change in SESR between consecutive 8 d intervals (p) within each crop management period (t) and for sample (k) falling within a soil texture class. P40 is the 40th percentile of the ΔSESR distribution values. P25 is the 25th percentile of the ΔSESR distribution. $\overline{\Delta\mathrm{SESR}}_{s,t,k}$ is the mean ΔSESR over the full candidate agricultural flash drought period (s) within each crop management period (t) and for sample (k) falling within a soil texture class. ∧ denotes the logical "AND" condition.

2.3.3 Determining differences in evaporative stress signals between years with and years without drought-induced crop losses prior to calibration

To determine differences in evaporative stress signals linked to years with and years without drought-induced crop losses, a comparison of the distribution of SESR values in two reference years was conducted, with one of the years having clear drought induced crop losses while the other year has no losses. These reference years were identified using the VHI-based drought-induced crop loss benchmark (Sect. 2.3.1). For each reference year, VHI and SESR time series for each sample location were extracted in their original 8 d resolution for the period from February to July and then grouped by soil texture class. The distribution of SESR values across crop management periods and soil texture classes are examined to establish whether these differ between years with drought-induced crop losses and years without such losses. Mann–Whitney U and Kolmogorov–Smirnov tests (Sawilowsky, 2005), are used to test differences found at the 5 % significance level ($p < 0.05$), as most SESR distributions deviated from normality according to the Shapiro–Wilk normality test (Ghasemi and Zahediasl, 2012). A complementary linear regression and Pearson correlation analysis between SESR and VHI was also conducted to confirm the discriminatory ability of SESR, with results provided in Fig. S1 in the Supplement.

2.3.4 Deriving and evaluating calibrated impact-informed SESR thresholds

The calibration aimed to identify optimal values of the SESR threshold ($\Theta_{t,k}$) that best separate years with from years without drought-induced crop losses. The calibration was performed from 2000 to 2013 using the original 8 d SESR observations from February to July and the VHI-based drought-induced crop losses as a benchmark at each sample location. SESR observations from August, which corresponds to the harvest period, were excluded from threshold optimisation because crops have reached physiological maturity, meaning late-season evaporative stress no longer impacts crop yield formation (Anderson et al., 2016; Verbist et al., 2018).

The 8 d SESR observations were stratified by month and soil texture classes without losing their original temporal resolution. These monthly threshold estimates were subsequently mapped to their corresponding crop management periods. Within each stratum, SESR observations were classified into positive and negative classes according to years with and without drought-induced crop losses, determined using the VHI-based agricultural benchmark (Sect. 2.3.1). As the number of SESR time series was imbalanced across soil textures given the spatial extent of these, inverse-frequency weighting was applied (Cao et al., 2019). Candidate drought onset thresholds were defined as SESR values ranging between the 2nd and 95th percentiles of the SESR distributions, with a step size of 0.01. A time step was classified as drought when the SESR value fell below the candidate onset threshold and as non-drought otherwise (note that the rapid intensification criteria P40 and P25, were retained unchanged as defined in Sect. 2.3.2 and applied during full event detection). The resulting drought and non-drought classifications were then compared with their corresponding positive or negative reference classes to compute precision and recall for each candidate threshold. Precision represents the proportion of correctly detected drought events (true positives, TP) among all events classified as drought, including false drought alarms (false positives, FP). Conversely, recall

(also known as hit rate) represents the proportion of correctly detected drought events (TP) among all observed events in the dataset, including missed events (false negatives, FN). Precision and recall involve a trade–off, as increasing recall generally leads to more false alarms and thus lower precision, while increasing precision may increase missed events. Higher precision is often important in operational drought warning systems because reducing excessive false alarms may improve user confidence (Takáts, 2007). Precision and recall values were used to derive the F_β score for each candidate threshold, with the F_β metric defined as:

$$F_\beta = \frac{(1+\beta^2)P.R}{\beta^2 P + R} \quad (4)$$

where P is precision, R is recall, and the F_β score represents an adjusted balance that weights P and R depending on the value of β. Lower β values (≤ 0.5) place greater emphasis on precision, whereas higher β values (≥ 0.5) favour recall in the F_β score. In this study, $\beta$was set to 0.3 to place greater emphasis on precision. This choice is consistent with stakeholders' preferences for minimising false alarms relative to missed drought-impact events (Guimarães Nobre et al., 2023). Candidate thresholds were evaluated using an empirical-utility maximisation approach (Nan et al., 2012), with optimal thresholds identified by maximising the F_β score.

To assess the stability of the calibrated thresholds, uncertainty was estimated using cluster-level bootstrapping (Padiyedath Gopalan et al., 2019) with 1000 replicates (Efron and Tibshirani, 1986). The bootstrap procedure resamples the SESR time series (February–July) for each location with replacement at the year level. The resulting distribution of thresholds are summarised using the 95 % confidence interval ($CI_{95\,\%}$). The calibrated thresholds were then compared with the literature-based thresholds to determine whether these provide gains in performance, and how these gains vary across soil textures and crop management periods. The comparison was based on performance metrics including precision, recall, false alarm rate (FAR), and discrimination metric such as Receiver Operating Characteristics Curve (ROC) and the corresponding Area Under Curve (AUC). Higher precision values (≥ 0.70) indicate fewer false drought detections, whereas higher recall values (≥ 0.70) indicate fewer missed drought-impact events. Lower FAR values (≤ 0.3) indicate fewer false alarm drought detections, whereas higher FAR values (≥ 0.5) indicate a higher frequency of false alarms. AUC values greater than 0.5 indicate that the thresholds provide discriminatory ability between years with and without drought-induced crop losses beyond what would be expected by chance (Marzban, 2004).

Calibrated thresholds were subsequently filtered, where thresholds were considered as skilful only when simultaneously having precision ≥ 0.70, discrimination (AUC) ≥ 0.60, and uncertainty ($CI_{95\,\%}$) ≤ 0.40. These criteria were chosen to approximate likely stakeholder preferences for reliable drought detection with limited false alarms, acceptable discrimination between years with and without drought-induced crop losses, and stable threshold estimates. If these criteria are not satisfied, the threshold remains the optimal threshold identified through the F_β maximisation procedure but is simply not retained as a skilful calibrated impact-informed SESR threshold.

2.3.5 Validating literature-based and calibrated impact-informed SESR thresholds against agricultural impact benchmarks

The validation step assessed how well the literature-based and calibrated impact-informed SESR thresholds identified flash drought events associated with drought-induced crop losses. Validation was performed only for the crop management periods and soil textures for which skilful thresholds were identified following calibration and was conducted over the 2014–2024 period using both agricultural benchmarks from the VHI (V1) and documented historical newspapers and reports (V2; see Sect. 2.3.1). Their agreement with the detected flash drought events was evaluated through hit rates. The hit rate, or recall, is calculated based on the years for which a flash drought coincided with a year in which agricultural impacts are reported. V1 is the hit rate established using the first benchmark based on VHI, while V2 is the hit rate established using the second benchmark.

3 Results

3.1 Differences in evaporative stress signals between years with and without crop losses

Boxplots of SESR distributions (Fig. 3), together with the statistical difference tests (see Fig. S2), illustrate how evaporative stress varies across crop management periods and soil textures between years with and years without drought-induced crop losses. During February and March, SESR distributions exhibit strong overlap in both medians and interquartile ranges (IQRs), indicating limited discrimination between conditions. From April onwards, differences begin to emerge, with these being clearest in May−July, when years with drought-induced crop losses consistently show lower SESR medians across all soil textures. This separation is weakest in coarse sandy soils, where IQRs remain large and mostly overlapping. In contrast, it is strongest in finer-textured soils (moderately fine clay-loam, fine clayey, and very expansive clayey), where a persistent downward shift in the median occurs without a corresponding increase in distributional spread. During June–July, separation further reveals a higher prevalence and greater magnitude of negative SESR values, particularly in fine-textured soils, indicating that the late period differences arise from both shifts in typical conditions (lower medians) and enhanced lower tail behaviour.

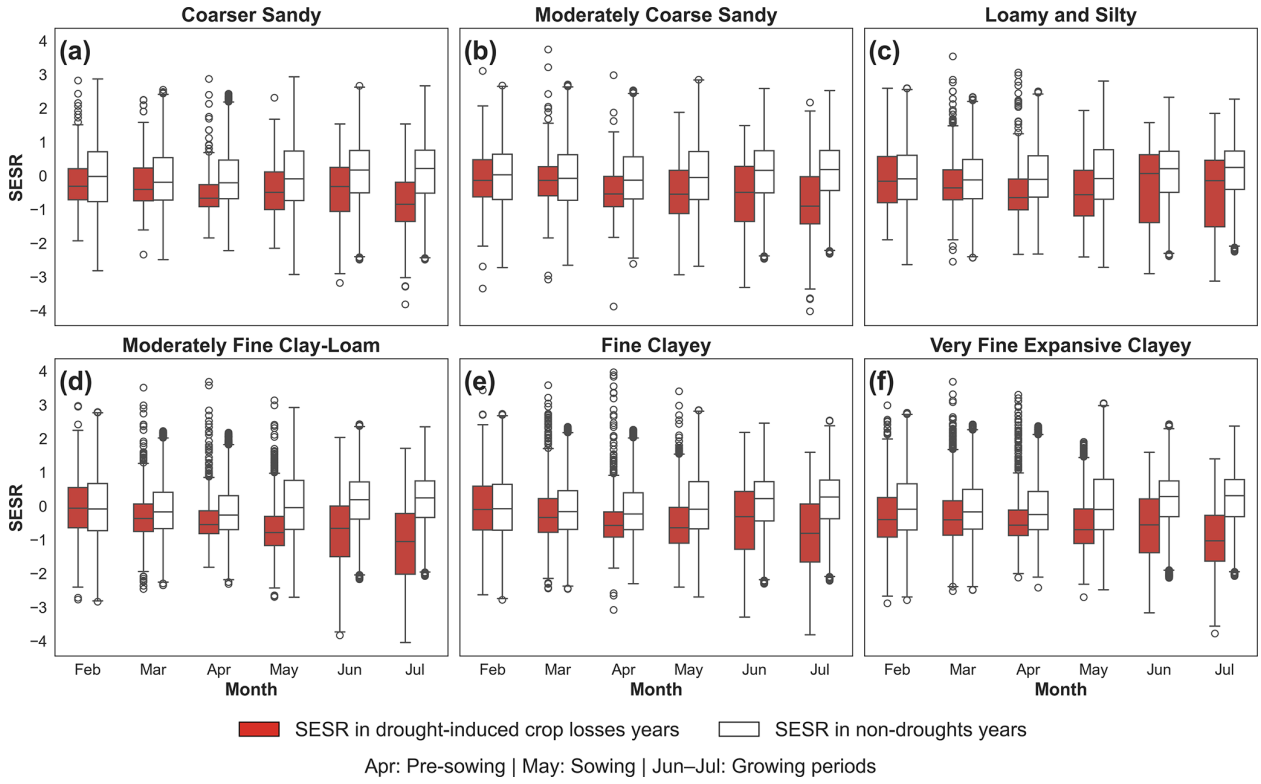


Figure 3. (a–f) Standardized Evaporative Stress Ratio (SESR) aggregated across crop management periods and soil texture classes at the sample locations for years with and without drought-induced crop losses.

The relatively low discrimination of SESR in sandy soils between years with and without drought-induced crop loss years can be explained by their high permeability and low water-holding capacity (Jabro et al., 2009; Wankmüller et al., 2024), which cause rapid responses to evaporative demand even in years without crop losses. Consistent with this behaviour, statistical tests show no significant differences in SESR between years for sandy soils (Fig. S2). The stronger discrimination observed in clay-rich soils is likely linked to their higher water retention capacity (Or and Lehmann, 2019; Sun et al., 2019), which allows evaporative stress signals to persist longer and enhances the contrast in SESR between drought-induced crop loss and no-drought years. Discrimination is supported by statistically significant differences ($p < 0.05$) in both tests (Fig. S2). Moreover, the upper and lower tails of the SESR distribution in these soils exhibit comparable lengths, indicating that the area experiences a balanced range of extreme transitions rather than being dominated exclusively by drying or wetting anomalies. This balance enables SESR to capture both the intensification and easing of evaporative stress, thereby supporting a more reliable identification of stress-related thresholds.

3.2 Calibrated impact-informed SESR thresholds across crop management period and soil textures

3.2.1 Performance and discrimination relative to literature-based thresholds

Figure 4 shows how the median performance metrics of precision, recall, False Alarm Rate (FAR) and F_β vary across the range of thresholds $\Theta_{t,k}$ (Eq. 3). For each crop management period and soil texture combination, the candidate threshold at which F_β reaches its maximun was selected as the optimal threshold. In each panel, the optimal threshold ($\Theta_{t,k}$) is indicated by a solid vertical line, with its value reported in the title, whereas the literature-based threshold is shown as a dotted vertical line for comparison. While Fig. 4 illustrates the overall behaviour of the metrics across the threshold range, the numerical values discussed below refer specifically to the values of the performance metrics at the optimal thresholds.

In all soil textures, higher values of the SESR thresholds increase recall and FAR and decrease precision. The metric combinations at the F_β maximum differ across soil textures and crop management periods. During the pre-sowing period (April), loamy and silty soils exhibit calibrated thresholds with high precision ($\approx$0.83) while retaining a recall of approximately ≈ 0.68, whereas coarse sandy soils show lower recall (≈ 0.43–0.66) and higher FAR (> 0.20). Dur-

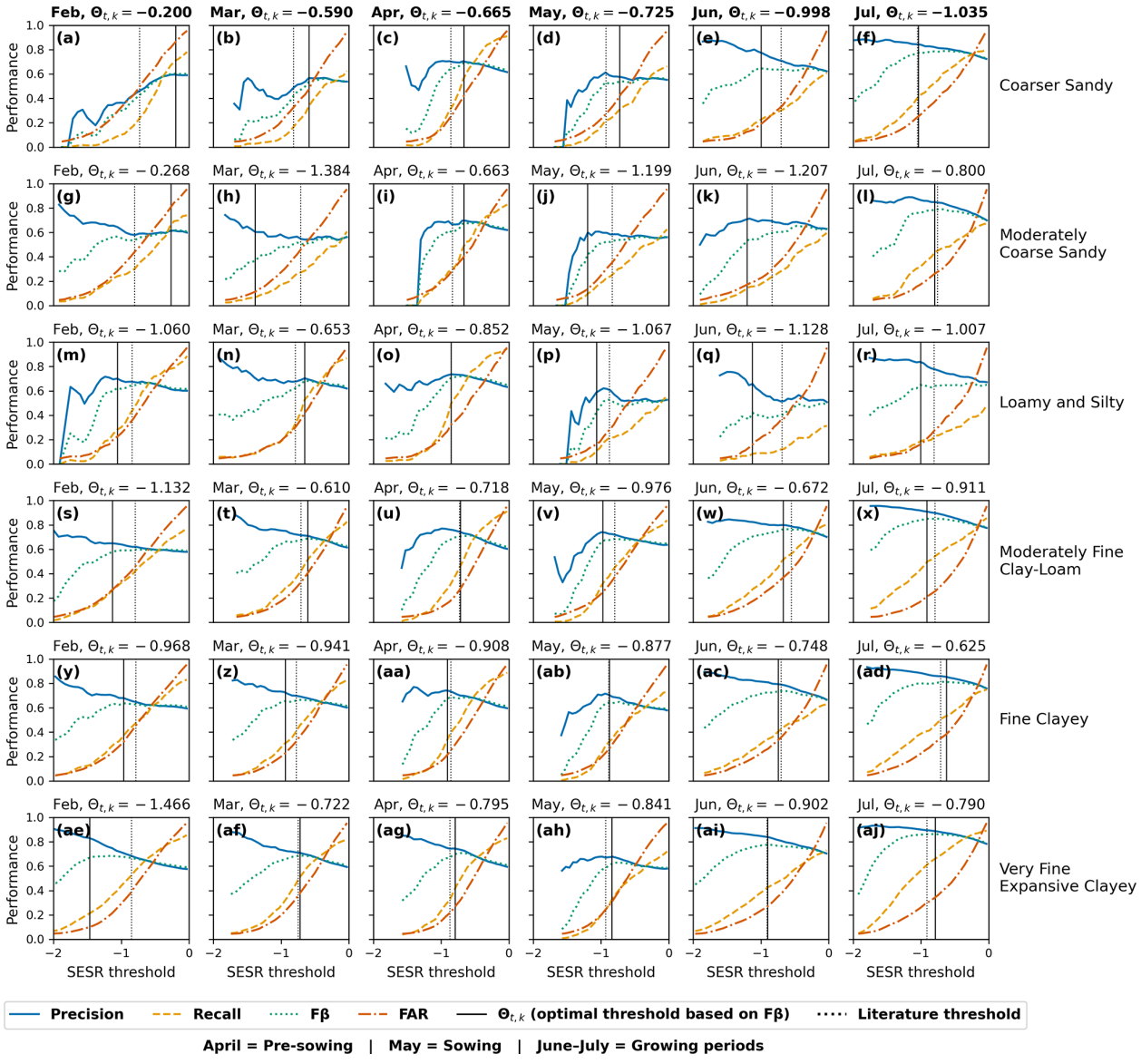


Figure 4. Median performance metrics of SESR thresholds across crop management periods and sample points for each soil texture, including precision, recall, F_β, and False Alarm Rate (FAR) evaluated over the full thresholds range. Solid vertical line denotes the optimal calibrated thresholds ($\Theta_{t,k}$), while the dotted vertical line shows reference thresholds from literature. Note that the z-score of the literature thresholds is derived from the empirical distribution of SESR.

ing the sowing period (May), most soils are characterised by calibrated thresholds with reduced recall (< 0.45) and FAR typically bellow 0.12, including moderately coarse sandy, loamy–silty, and clay-loam soils. In contrast, during the growing period (June–July), calibrated thresholds in nearly all soil textures have high precision (> 0.84) and low FAR (< 0.12), while recall varies across soils, ranging from approximately 0.32 in coarser sandy soils to above 0.68 in fine and very fine clayey soils. Compared with the literature-based SESR thresholds, the calibrated thresholds generally correspond to more favourable combinations of precision, recall, FAR, and F_β during the growing period (June–July). These improvements are most evident in moderately fine clay-loam, fine clayey, and very fine expansive clayey soils, where the optimal thresholds are associated with improved recall–FAR trade-offs while maintaining high precision. In contrast, both threshold methods exhibit relatively similar performance in loamy–silty soils, whereas lower discrimination is observed in both methods in coarse sandy and moderately coarse sandy soils, particularly during the pre-sowing and sowing periods.

Figure 5 further shows that these differences translate into stronger discrimination between years with and without drought-induced crop losses. During the growing period, op-

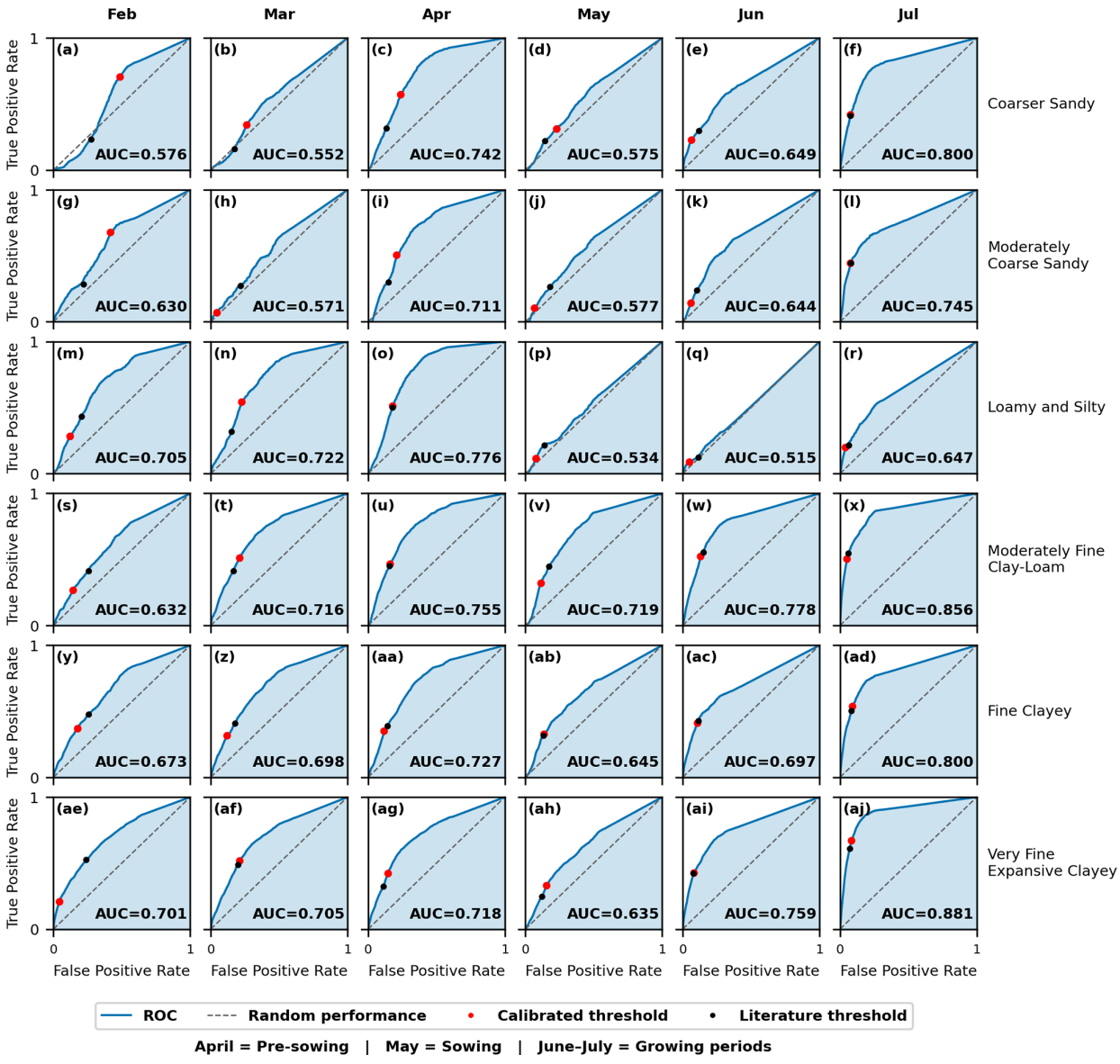


Figure 5. Median Receiver-Operating Characteristics Curve (ROC) values across crop management periods and sample points for each soil textures.

timal thresholds in finer-textured soils commonly correspond to higher true positive rates at comparable or lower false positive rates than the literature-based thresholds. Lower discrimination is mainly observed during the pre-sowing (April) and sowing (May) periods for several soil textures, including coarse sandy, moderately coarse sandy, and loamy–silty soils (AUC ≤ 0.70). In contrast, the highest discrimination is consistently observed during the growing period (June–July) across fine and very fine clayey soil textures, with AUC values commonly exceeding 0.80 and in some cases surpassing 0.90.

3.2.2 Uncertainty of calibrated SESR thresholds and selection of calibrated impact-informed SESR thresholds

Figure 6 shows the uncertainty in the optimal SESR-based thresholds across crop management periods and soil textures, expressed by the $CI_{95\,\%}$. Cells with a black outline indicate soil texture–month combinations in which the thresholds simultaneously satisfy the: precision (≥ 0.70), AUC (≥ 0.60), and $CI_{95\,\%} \leq 0.40$. Only these thresholds were retained for validation. Threshold uncertainty varies across both crop management periods and soil textures. Sandy soils (coarse sandy and moderately coarse sandy) exhibit the highest $CI_{95\,\%}$ ranges during the selected period. In contrast, in-

termediate and fine-textured soils show lower $CI_{95\,\%}$ range. Skilful thresholds are identified for loamy and silty soils during March and April (pre-sowing period), for moderately fine clay-loam soils during April and June–July (growing period), and for very expansive clayey soils from March through July (growing period). Fine clayey soils exhibited intermediate uncertainty, exceeding the selection threshold in most months. However, skilful thresholds were successfully identified during the growing period (June−July), where uncertainty remained within acceptable limits ($CI_{95\,\%} \leq 0.40$. The variability underlying these $CI_{95\,\%}$ values are shown in Fig. S3, where the distribution illustrates the repeated estimates of the optimal SESR thresholds obtained across the bootstrap replicates rather than alternative optimal thresholds.

3.2.3 Application of calibrated impact-informed SESR thresholds to detect agricultural flash drought

Figure 7 illustrates an agricultural flash drought (AFD) event in 2014 in moderately fine clay-loam soil at one of the sample points. Panel (a) shows the SESR trajectory (black line) together with the calibrated threshold (red dashed line). From mid-May to early July, SESR dropped below the calibrated threshold for 49 consecutive days. Panel (b) shows the ΔSESR during the event. Rapid intensification is confirmed as consecutive ΔSESR values remained below the 40th percentile, with only one exception allowed, which is marked here with an orange circle. The mean (μ) of the ΔSESR across the event also remains below the 25th percentile, reinforcing its classification as an AFD. In the figure, the actual μ (ΔSESR) and the 40th and 25th percentiles of the time series are shown to better illustrate the example. Detection therefore requires both sustained low SESR and rapid intensification, with the calibrated SESR threshold governing the event onset in this example.

3.3 Validation of literature-based and calibrated impact-informed SESR thresholds against agricultural benchmarks

Figure 8 illustrates years in which flash droughts are detected using calibrated thresholds and literature-based thresholds for the validation period (2014–2024), and how these align against years with crop losses. This shows that flash drought events that are detected using calibrated thresholds appear in more years and across more soil textures than those detected using literature-based thresholds. In moderately fine clay-loam, fine clayey, and very fine expansive clayey soils, calibrated threshold detections are present in several years in which crop losses are also shown. In contrast, detections based on literature thresholds are absent or limited to fewer years for these same soils. In loamy and silty soils, both calibrated and literature-based flash drought detections occur less frequently, and several years with crop losses do not show a corresponding flash drought detection. Across all soil textures, there are also years in which flash drought detections occur without corresponding crop losses, and years in which crop losses occur without flash drought detections.

Figure 9 summarises the hit rates between flash droughts detected using literature-based (left half) or calibrated impact-informed (right half) thresholds versus crop losses identified via VHI (upper half) and reports (lower half). For all soil textures, hit rates are zero or low during the pre-sowing and sowing periods. During the growing period (June–July), calibrated thresholds yield consistently higher hit rates than literature-based thresholds across all soil textures, with the highest values observed in moderately fine clay-loam and fine clayey soils. In contrast, hit rates associated with literature-based thresholds remain low across all periods and soil textures.

4 Discussion

4.1 Relevance of SESR in detecting agricultural flash droughts

Results show that the Standardized Evaporative Stress Ratio (SESR) captures a coherent signal of higher evaporative stress during years in which crop losses are observed (Fig. 3), as also indicated by contrasts in the SESR-VHI relationship between non-drought and drought years (Fig. S1). This indicates that SESR is coherent with vegetation stress during years with confirmed crop losses. This behaviour is consistent with the mechanism whereby vegetation becomes increasingly sensitive to evaporative stress once soil moisture constraints emerge, whereas under non-limiting conditions changes in evaporative demand do not translate into physiological stress (Anderson et al., 2016; Hobbins and Huntington, 2016; Kozlowski, 1968). However, translating this signal into an indicator of agricultural flash drought depends on how the onset threshold is defined within the detection approach (Sect. 2.3.2). Literature-based thresholds are defined solely by the statistical properties of the SESR distribution (Christian et al., 2019), whereas calibrated impact-informed thresholds are constrained by the occurrence of observed crop losses (see Sect. 2.3.1, 2.3.2, and 2.3.4). Although calibrated thresholds are derived separately for each crop management period and soil texture, they approach similar values to the literature-based thresholds for a limited number of cases (Fig. 4), but this similarity represents a numerical coincidence.

The practical implications of calibrated, impact-informed thresholds are reflected in the higher hit rates compared with those found with literature-based thresholds (Fig. 9). This is particularly relevant for agricultural flash drought detection because the detected occurrence of flash drought may then not correspond to crop losses (Halwatura et al., 2017; Teleubay et al., 2025; Walker et al., 2024), particularly when

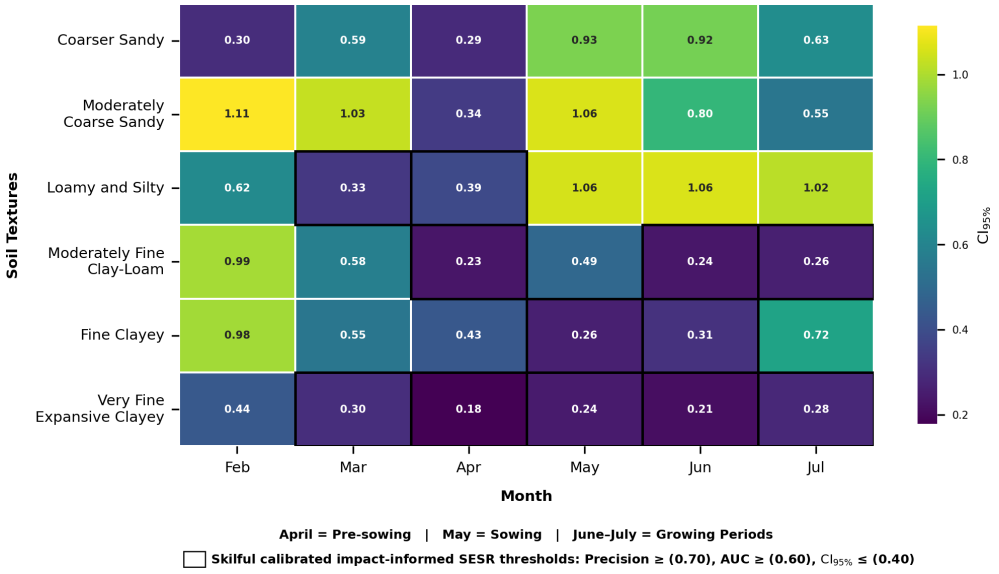


Figure 6. Uncertainty of optimal calibrated thresholds by crop management periods and soil textures. The black outlined cells show the calibrated impact-informed SESR thresholds that simultaneously satisfy criteria for: precision, AUC, and $CI_{95\,\%}$.

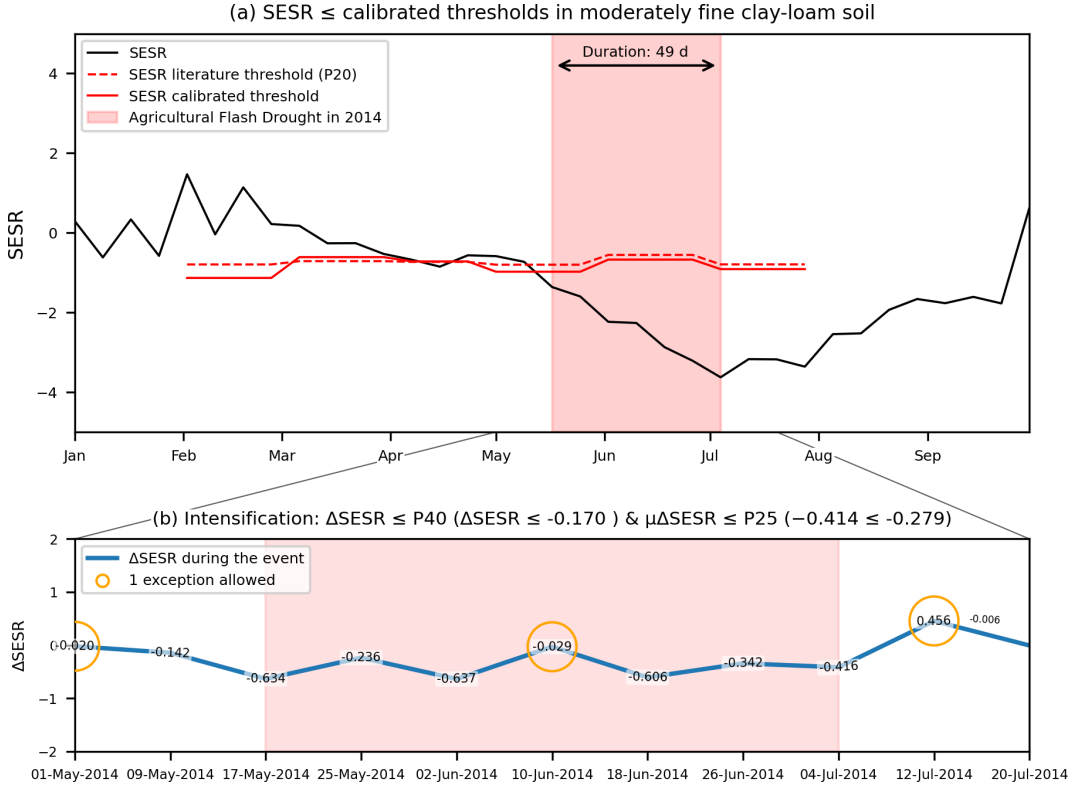


Figure 7. Time-series schematic showing how calibrated SESR thresholds and rapid intensification criteria are used to detect an agricultural flash drought in 2014. **(a)** SESR evolution relative to the calibrated threshold ($\Theta_{t,k}$) and the fixed literature-based threshold (SESR $\leq$ P20; Christian et al., 2019). The shaded period indicates the detected agricultural flash drought, which begins when SESR falls below the calibrated threshold (on 17 May) and persists while rapid intensification criteria are satisfied. **(b)** Rapid intensification criteria evaluated through consecutive changes in SESR (ΔSESR $\leq$ P40, allowing at most one non-consecutive exception marked by the orange circle) and the mean change across the entire event duration ($\mu\,\Delta$SESR $\leq$ P25).

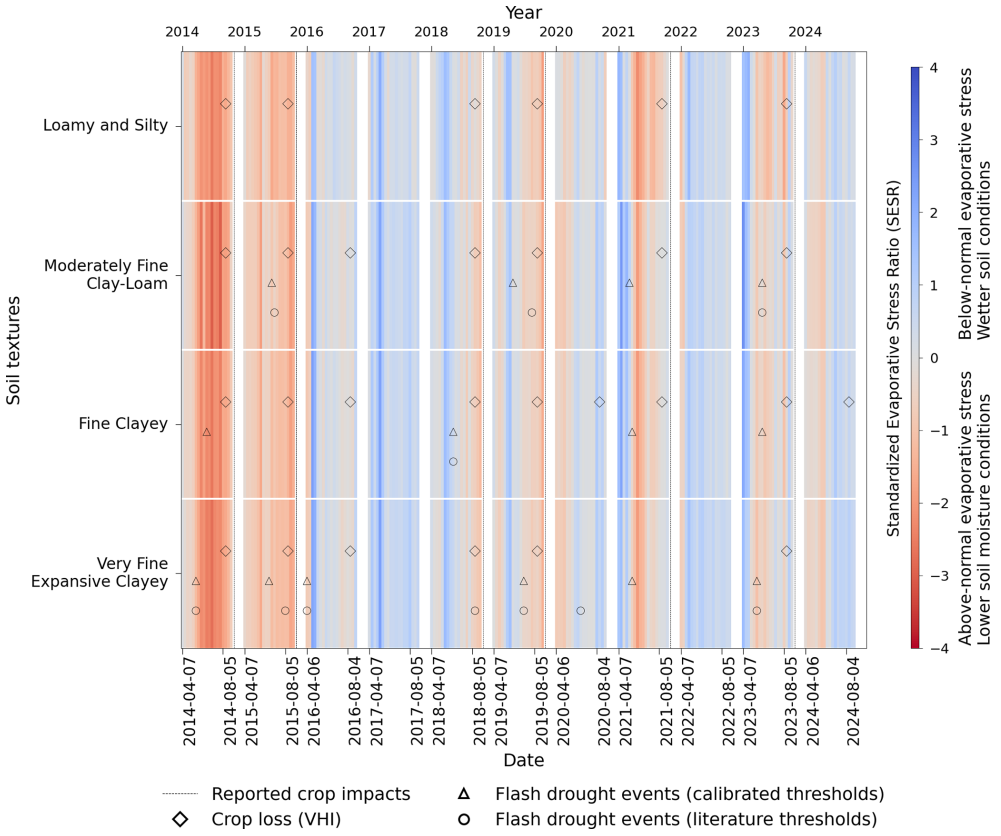


Figure 8. Temporal alignment of flash droughts events and crop losses identified via VHI and newspapers/reports. The 8 d SESR time series for each soil texture is shown as the background over the evaluation period. Flash drought events detected using calibrated impact-informed and literature-based thresholds, together with reported crop losses, are overlaid.

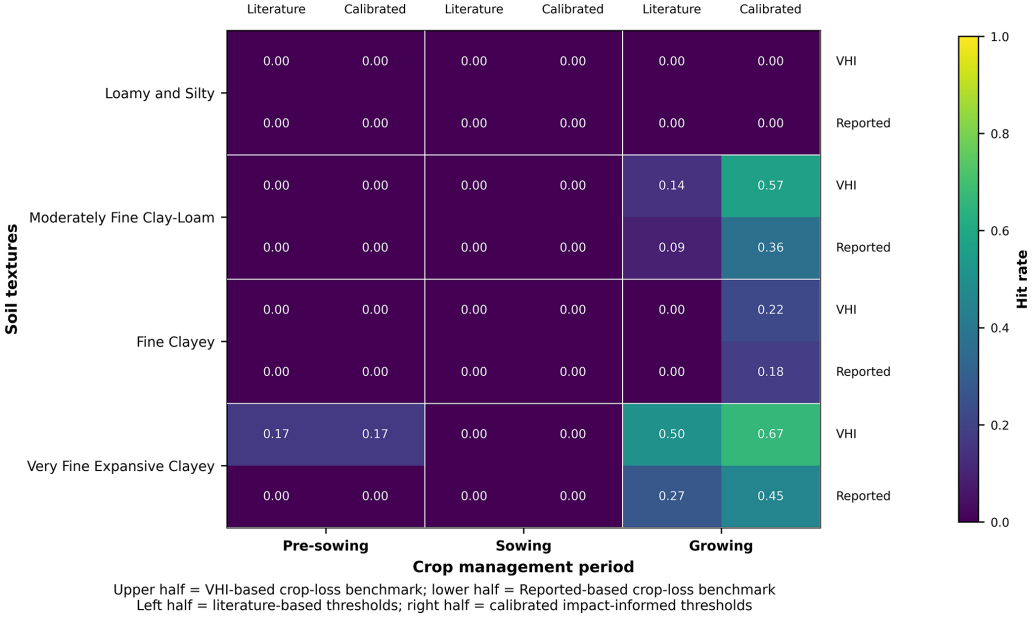


Figure 9. Hit rates between flash droughts detected using literature-based or calibrated impact-informed thresholds versus crop losses detected identified using Vegetation Health Index (VHI) and reports benchmarks.

it is detected to occur outside pre-sowing, sowing and growing periods relevant to crop production (Bucheli et al., 2021). In rainfed systems, where producers face tight cost–loss margins and varying levels of risk aversion (Linés et al., 2018) impact-informed calibration can help ensure that early warnings represent conditions associated with agricultural impacts (Halwatura et al., 2017). In this sense, impact-informed thresholds align directly with impact-based forecasting, the core principle of which is to link hazard signals to locally relevant impacts to support meaningful early warning and decision-making (McEwen et al., 2021; Shyrokaya et al., 2024).

4.2 Behaviour of calibrated SESR thresholds across soil textures and crop management periods to detect agricultural flash droughts

The response of calibrated SESR thresholds across soil textures and crop management periods shows that flash drought detection depends on both the temporal evolution of evaporative stress and the capacity of each soil texture to store and release moisture over time. In the Dry Corridor of Nicaragua, high atmospheric demand during the dry season (Fig. 2), followed by the transition to the rainy season (van der Zee Arias et al., 2012), produces rapid fluctuations in soil moisture (Son et al., 2018). Because local maize and bean production relies almost entirely on precipitation (van der Zee Arias et al., 2012), these soil moisture fluctuations translate into short-term vegetation stress that is captured by the lower SESR values observed during drought years (Figs. 3 and S2).

Coarse and moderately coarse sandy soils, with rapid drainage and low water–holding capacity (Jabro et al., 2009; Wankmüller et al., 2024), generate short-lived and highly variable evaporative stress, making SESR signals less persistent and less clearly associated with crop losses. This is reflected in the weak discrimination of SESR distributions between years with and years without identified crop losses (Fig. 3a, b) and by the high uncertainty of the resulting calibrated thresholds (Fig. 6). In contrast, clay-rich soils, characterised by greater water retention and slower drainage (Jabro et al., 2009), allow evaporative stress to persist over longer periods (Suliman et al., 2024; Wankmüller et al., 2024), which is reflected in more stable calibrated thresholds in clay soil class during the growing period (Fig. 6). Loamy–silty soils, which have intermediate porosity and water–holding capacity (Ma et al., 2015), exhibit a more mixed behaviour. Although they show clear separation of the SESR signal during pre-sowing, sowing, and growing periods (Fig. 3c), this translates into skilful calibrated impact-informed SESR thresholds only in March and during the pre-sowing period in April (Fig. 6). These contrasts suggest that SESR-based detection is most reliable where soil moisture conditions allow evaporative stress signals to persist over a longer period to reflect sustained crop impacts, whereas rapidly draining soils reduce the operational usefulness of SESR as a standalone indicator.

The usefulness of calibrated impact-informed SESR thresholds is governed not only by soil texture but also by the seasonal progression of evaporative stress across crop management periods (Son et al., 2018). During the dry season months (such as March and April) that precede the sowing period, high evaporative stress dominates the SESR signal (Fig. 2), producing large variability that often reflects background seasonal drying rather than short-term stress anomalies associated with agricultural impacts (Hobbins and Huntington, 2016; Noguera et al., 2022; Otkin et al., 2018). Because these high evaporative drying effects all years, SESR distributions between years with and without crop losses overlap during April and May (Fig. 3), which reduces threshold reliability (Fig. 6) and results in elevated false alarm rates (FAR; Fig. 4) before precipitation becomes established (Fig. 1c).

Once precipitation begins to moderate evaporative stress (Fig. 2) during the sowing period in May and during the subsequent growing period in June–July for maize and beans (Fig. 1c), soil moisture is replenished more regularly (Son et al., 2018). This reduces the gap between ET and PET (Hobbins et al., 2019) and short-term variability in SESR (Noguera et al., 2022). Under these more stable conditions, SESR signals become more distinguishable between drought-induced crop loss and non-drought years (Fig. 3), allowing SESR signals to more clearly reflect crop-relevant soil moisture deficits (Anderson et al., 2016) in the soil-crop management period combinations where skilful detection is observed (Fig. 6). This seasonal transition modifies the SESR signals, but ROC results indicate that skilful discrimination does not increase uniformly after the onset of rainfall (Fig. 5). Instead, skill emerges only in specific soil texture and crop management period combinations, consistent with the combined influence of seasonal moisture dynamics and soil water–holding capacity. Operationally, this implies that SESR-based flash drought monitoring in dryland agricultural systems should focus on the specific soil–crop management period combinations where skilful detection is observed, rather than applying a uniform approach across all soil textures and crop management periods.

4.3 Operational relevance and limitations of calibrated SESR thresholds for flash drought monitoring and management

The calibrated thresholds reveal context-dependent limitations that must be recognised when integrating SESR into operational drought monitoring. In sandy soils, SESR shows limited ability to distinguish anomalous evaporative stress from background dryness signals (Hobbins and Huntington, 2016; Jabro et al., 2009), resulting in low detection skill and high uncertainty in calibrated thresholds. In contrast, skilful thresholds (Fig. 6) occur predominantly in clay-

rich soils, which account for around 90 % of the study area (Fig. 1a), during the pre-sowing, sowing, and growing periods (Fig. 1c), whereas in loamy–silty textures they occur only during the pre-sowing period. This spatial and temporal concentration of skilful thresholds indicates that SESR provides operational value only for specific combinations of crop management period and soil texture, and that good performance cannot be assumed outside these domains. Therefore, SESR-based monitoring may not be suitable as a uniformly applied early warning tool across all periods and soils, but rather as a selective component restricted to the conditions where calibrated thresholds demonstrate stability and skill. Even in these settings, SESR-based detections would benefit from verification using complementary information, such as soil moisture indicators, land surface temperature or field-based agronomic observations, to confirm or filter detections (Torelló-Sentelles and Franzke, 2022), and to avoid overinterpreting SESR signals, as documented in previous studies in dryland regions such as in Central America (Kibler et al., 2023; Quichimbo et al., 2021; Sun et al., 2019). Additionally, the operational relevance of SESR thresholds depends on the trade-off between missed events and false alarms that local governments, managers, and farmers are willing to accept (Guimarães Nobre et al., 2023). The choice of the optimal threshold based on the maximum value of F_β is conditioned by the parameter β, which determines how the system balances missed events and false alarms (Gallear et al., 2025). In this study, thresholds were selected to favour precision, consistent with a context where false alarms carry high costs (Guimarães Nobre et al., 2019) and institutional response capacity is limited. Under this configuration ($\beta = 0.3$), the optimal threshold shifts towards more negative values, reducing false alarms (FAR) while increases the likelihood of missing early flash drought development. When $\beta = 1$, which gives greater relative weight to recall than $\beta = 0.3$, thresholds shift toward less negative SESR values, increasing detection under weaker stress and thereby increasing FAR. This behaviour of SESR is consistent with findings for other drought indicators (Halwatura et al., 2017; Gallear et al., 2025; Torelló-Sentelles and Franzke, 2022). As discussed in the literature, decision-makers often avoid acting when uncertainty is high, because the penalties associated with false alarms are visible, whereas the benefits of early actions are less immediately apparent (Bailey, 2012).

These decision rules ultimately depend on what local decision-makers prioritise (Guimarães Nobre et al., 2019; Linés and Werner, 2025; Lopez and Haines, 2017), and in the rainfed Central America Dry corridor, this statistical trade-off translates directly into an economic trade-off. By mid-May, farmers have already committed financial resources – loans, fertiliser, and labour (van der Zee Arias et al., 2012). Because flash droughts typically evolve over timescales comparable to the sowing period (~ 30 d), prioritising precision may reduce false alarms (Gallear et al., 2025) but delay response, thus limiting the opportunity to reschedule planting or implement mitigation (Solh and van Ginkel, 2014). This delay effectively narrows the window for early action between the detection of emerging drought conditions and the point at which preventive agricultural measures can still be implemented (Fuganti et al., 2020). Conversely, favouring recall in May may increase early detection even under weak stress signals (Halwatura et al., 2017) and enable preventive action, but at potentially high implementation costs. In line with principles of impact-based forecasting (Shyrokaya et al., 2024), a more appropriate strategy would be to redefine the objective function according to economic risk (Bailey, 2012; Portele et al., 2021; Salmoral et al., 2019) and cost–loss analysis (Zhu et al., 2002), while incorporating the participation of stakeholders (Linés et al., 2018) rather than relying purely on statistical criteria (McEwen et al., 2021). Although this study adjusted the optimal thresholds to account for spatial and temporal variability across crop management periods and soil textures, a fully operational deployment would require extending this approach to explicitly account for economic risk, stakeholder priorities, and decision-making constraints.

5 Conclusions

In this study, a context-specific threshold calibration was tested to improve the spatial and temporal detection of agricultural flash drought conditions in support of drought monitoring and management. The study was conducted in the Central American Dry Corridor, a dryland region in Nicaragua that is representative of rainfed agricultural systems exposed to short-lived but intense evaporative stress, as found in many tropical drylands worldwide. The study uses the Standardized Evaporative Stress Ratio (SESR) to calibrate SESR thresholds for flash drought detection using benchmarks of observed drought-induced crop loss impacts. Calibrated SESR thresholds were evaluated across crop management periods and soil textures. The conclusions are summarised below:

- In this dryland study area, although SESR showed signals of evaporative stress during years with drought-induced crop losses, literature-based thresholds did not translate these signals into detections associated with agricultural impacts. These thresholds showed less favourable performance, particularly in discriminating years with reported drought-induced crop losses from years without losses. As a result, literature-based thresholds showed limited suitability for operational flash drought monitoring in the study region.

- Calibrated thresholds suggest that the detectability of agriculturally relevant flash drought conditions using SESR depends both on crop management periods and soil textures. Skilful thresholds could not be found in sandy soils, where rapid soil moisture fluctuations as-

sociated with high permeability and low water–holding capacity limit the persistence of evaporative stress signals even in years with drought-induced crop losses. In contrast, clay-rich soils exhibited skilful thresholds during specific crop management periods, although these periods differ for individual clay-rich soil classes. Loamy–silty soils showed intermediate behaviour, with skilful thresholds found only in March and during the pre-sowing period in April. These results indicate that SESR-based flash drought detection cannot be generalised uniformly across space or time but instead varies with soil texture and associated soil hydraulic properties, as well as the seasonal evolution of evaporative stress across crop management periods.

– Validation against the agricultural benchmarks confirms that calibrated impact-informed thresholds detect flash drought conditions more frequently in years that also exhibit drought-induced crop losses than literature-based thresholds. However, detections also occurred in some years without reported losses, while reported losses were missed in others. This indicates that calibrated SESR thresholds can provide operationally relevant detections, but these are constrained to specific soil texture–crop management period combinations. More broadly, these findings support ongoing efforts towards impact-based drought monitoring by showing that, in this dryland context, physically based indicators such as SESR require calibration against observed agricultural impacts to enhance their operational relevance for agricultural decision making.

Further work is needed to generalise and deepen these findings. As the approach itself is generalisable, future research should test the transferability and detection skill of calibrated impact-informed thresholds in other dryland regions and cropping systems. Additionally, further research should explore adding complementary variables in settings where SESR alone does not sufficiently discriminate impact-relevant stress conditions. Finally, threshold selection cannot be reduced to mechanical optimisation of statistical metrics since effective operational use requires explicit consideration of economic risk, stakeholder priorities, and the asymmetric consequences of missed events and false alarms. Incorporating these considerations can help SESR-based alerts support timely, informed, and context-appropriate decision-making for farmers and institutions.

Code and data availability. The data and code are available upon reasonable request. The data include the processed benchmark datasets used for calibration and validation. The code covers all procedures described in Sects. 2.1 (Remote sensing data preparation), 2.3.2 (Detecting agricultural flash droughts), and 2.3.4–2.3.5 (Deriving, evaluating, and validating calibrated impact-informed SESR thresholds). The original datasets used in this study are publicly available from their repositories:

- Evapotranspiration and Potential Evapotranspiration from MYD16A2GF dataset: https://doi.org/10.5067/MODIS/MYD16A2GF.061 (Running et al., 2021),
- the Vegetation Health Index (VHI) dataset: https://www.fao.org/giews/earthobservation/access.jsp?lang=en (FAO, 2014),
- the cropland product: https://doi.org/10.5067/COMMUNITY/LGRIP/LGRIP30.001 (Teluguntla et al., 2023).

Qualitative drought impact reports were compiled from:

- GIEWS (Global Information and Early Warning System on Food and Agriculture): https://www.fao.org/giews/reports/giews-updates/en/ (last access: 27 January 2024),
- FEWS NET (Famine Early Warning Systems Network): https://fews.net/ (last access: 27 January 2024),
- EM-DAT (The International Disaster Database: https://www.emdat.be/ (last access: 27 January 2024).

Supplement. The supplement related to this article is available online at https://doi.org/10.5194/nhess-26-6137-2026-supplement.

Author contributions. Ingrid Ubeda-Trujillo: conceptualisation (lead), methodology (lead), investigation (lead), formal analysis (lead), data curation and coding (lead), visualisation (lead), Writing – original draft, review and editing (lead), funding acquisition (lead). Micha Werner: conceptualisation (lead), methodology (lead), supervision (lead), and writing – review (lead) and editing (supporting). Claudia Bertini: conceptualisation (supporting), methodology (supporting), supervision (supporting), and writing – review (lead) and editing (supporting). Miriam Coender-Gerrits: conceptualisation (supporting), methodology (supporting), supervision (supporting), Graham Jewitt: conceptualisation (supporting), methodology (supporting), supervision (supporting), funding acquisition (lead). The first draft was written by Ingrid U-T, and all authors commented on previous versions of the manuscript.

Competing interests. The contact author has declared that none of the authors has any competing interests.

Disclaimer. Publisher's note: Copernicus Publications remains neutral with regard to jurisdictional claims made in the text, published maps, institutional affiliations, or any other geographical representation in this paper. The authors bear the ultimate responsibility for providing appropriate place names. Views expressed in the text are those of the authors and do not necessarily reflect the views of the publisher.

Acknowledgements. Ingrid Ubeda-Trujillo thanks the Schlumberger Foundation Faculty for their financial support.

Financial support. This work was financially supported by the Schlumberger Foundation Faculty for the Future Fellowship Program.

Review statement. This paper was edited by Brunella Bonaccorso and reviewed by two anonymous referees.

References

Anderson, M. C., Zolin, C. A., Sentelhas, P. C., Hain, C. R., Semmens, K., Tugrul Yilmaz, M., Gao, F., Otkin, J. A., and Tetrault, R.: The evaporative stress index as an indicator of agricultural drought in Brazil: an assessment based on crop yield impacts, Remote Sens. Environ., 174, 82–99, https://doi.org/10.1016/j.rse.2015.11.034, 2016.

Bailey, R.: Famine early warning and early action: the cost of delay. Chatham House, London, 24 pp., https://www.chathamhouse.org/sites/default/files/public/Research (last access: 8 November 2023), 2012.

Basara, J. B., Christian, J. I., Wakefield, R. A., Otkin, J. A., Hunt, E. H., and Brown, D. P.: The evolution, propagation, and spread of flash drought in the Central United States during 2012, Environ. Res. Lett., 14, 084025, https://doi.org/10.1088/1748-9326/ab2cc0, 2019.

Bucheli, J., Dalhaus, T., and Finger, R.: The optimal drought index for designing weather index insurance, Eur. Rev. Agric. Econ., 48, 573–597, https://doi.org/10.1093/erae/jbaa014, 2021.

Buitink, J., van Hateren, T. C., and Teuling, A. J.: Hydrological system complexity induces a drought frequency paradox, Front. Water, 3, 640976, https://doi.org/10.3389/frwa.2021.640976, 2021.

Cao, K., Wei, C., Gaidon, A., Arechiga, N., and Ma, T.: Learning imbalanced datasets with label-distribution-aware margin loss, Adv. Neural Inf. Process. Syst., 32, 1567–1578, 2019.

Christian, J. I., Basara, J. B., Otkin, J. A., Hunt, E. D., Wakefield, R. A., Flanagan, P. X., and Xiao, X.: A methodology for flash drought identification: application of flash drought frequency across the United States, J. Hydrometeorol., 20, 833–846, https://doi.org/10.1175/JHM-D-18-0198.1, 2019.

DGOT–INETER: Atlas nacional de suelos de la República de Nicaragua, Managua, Nicaragua, https://www.ineter.gob.ni/mapa/pub/atlassuelo/1erAltasNacionaldeSuelos.pdf (last access: 8 November 2025), 2024.

Edris, S. G., Basara, J. B., Christian, J. I., Hunt, E. D., Otkin, J. A., Salesky, S. T., and Illston, B. G.: Analysis of the critical components of flash drought using the standardized evaporative stress ratio, Agric. For. Meteorol., 330, 109288, https://doi.org/10.1016/j.agrformet.2022.109288, 2023.

Efron, B. and Tibshirani, R.: Bootstrap methods for standard errors, confidence intervals, and other measures of statistical accuracy, Stat. Sci., 1, 54–75, https://doi.org/10.1214/ss/1177013815, 1986.

FAO: Vegetation health index near real time (Global – dekadal – 1 km) – ASIS (raster), FAO, https://www.fao.org/giews/earthobservation/access.jsp?lang=en (last access: 27 January 2024), 2014.

Fuganti, G., Minelli, M., and Rojas, O.: Practical guidelines for early warning–early action plans on agricultural drought, FAO, Rome, Italy, https://openknowledge.fao.org/items/dd8ad74b-8c2f-40e6-b899-62e52d2aad07 (last access: 8 November 2023), 2020.

Gallear, J. W., Valadares Galdos, M., Zeri, M., and Hartley, A.: Evaluation of machine learning approaches for large-scale agricultural drought forecasts to improve monitoring and preparedness in Brazil, Nat. Hazards Earth Syst. Sci., 25, 1521–1541, https://doi.org/10.5194/nhess-25-1521-2025, 2025.

Ghasemi, A. and Zahediasl, S.: Normality tests for statistical analysis: a guide for non-statisticians, Int. J. Endocrinol. Metab., 10, 486–489, https://doi.org/10.5812/ijem.3505, 2012.

Gou, Q., Zhu, Y., Lü, H., Horton, R., Yu, X., Zhang, H., Wang, X., Su, J., Liu, E., Ding, Z., Wang, Z., and Yuan, F.: Application of an improved spatio-temporal identification method of flash droughts, J. Hydrol., 604, 127224, https://doi.org/10.1016/j.jhydrol.2021.127224, 2022.

Gu, Y., Wylie, B. K., Howard, D. M., Phuyal, K. P., and Ji, L.: NDVI saturation adjustment: a new approach for improving cropland performance estimates in the Greater Platte River Basin, USA, Ecol. Indic., 30, 1–6, https://doi.org/10.1016/j.ecolind.2013.01.041, 2013.

Guimarães Nobre, G., Davenport, F., Bischiniotis, K., Veldkamp, T., Jongman, B., Funk, C. C., Husak, G., Ward, P. J., and Aerts, J. C. J. H.: Financing agricultural drought risk through ex-ante cash transfers, Sci. Total Environ., 653, 523–535, https://doi.org/10.1016/j.scitotenv.2018.10.406, 2019.

Guimarães Nobre, G., Pasqui, M., Quaresima, S., Pieretto, S., and Lemos Pereira Bonifácio, R. M.: Forecasting, thresholds, and triggers: towards developing a forecast-based financing system for droughts in Mozambique, Clim. Serv., 30, 100344, https://doi.org/10.1016/j.cliser.2023.100344, 2023.

Halwatura, D., McIntyre, N., Lechner, A. M., and Arnold, S.: Capability of meteorological drought indices for detecting soil moisture droughts, J. Hydrol.: Reg. Stud., 12, 396–412, https://doi.org/10.1016/j.ejrh.2017.06.001, 2017.

Hobbins, M., Dewes, C., and Huntington, J. L.: Evaporative demand: dynamics and opportunities in drought early warning, monitoring, and vulnerability assessment, in: Proceedings of the Sixth Interagency Conference on Research in the Watersheds, DRI, Shepherdstown, USA, 211, https://doi.org/10.2737/SRS-GTR-243, 2019.

Hobbins, M. T. and Huntington, J. L.: Evapotranspiration and evaporative demand, in: Handbook of applied hydrology, edited by: Singh, V. P., 2nd edn., McGraw-Hill Education, New York, USA, 42.1–42.18, ISBN 978-0-07-183509-1, https://www.researchgate.net/publication/309682507_Evapotranspiration_and_evaporative_demand (last access: 8 November 2024), 2016.

INETER, ANA, UNI, and GIZ-PROATAS: Cuencas Hidrográficas de Nicaragua bajo la metodología Pfafstetter, 2014. https://cira.unan.edu.ni/wp-content/uploads/2016/07/Album-Cuencas-Nic-Revisado_ANA.pdf (last access: 8 November 2025), 2014.

Jabro, J. D., Evans, R. G., Kim, Y., and Iversen, W. M.: Estimating in situ soil–water retention and field water capac-

ity in two contrasting soil textures, Irrig. Sci., 27, 223–229, https://doi.org/10.1007/s00271-008-0137-9, 2009.

Kibler, C. L., Trugman, A. T., Roberts, D. A., Still, C. J., Scott, R. L., Caylor, K. K., Stella, J. C., and Singer, M. B.: Evapotranspiration regulates leaf temperature and respiration in dryland vegetation, Agric. For. Meteorol., 339, 109560, https://doi.org/10.1016/j.agrformet.2023.109560, 2023.

Kogan, F. N.: Application of vegetation index and brightness temperature for drought detection, Adv. Space Res., 15, 91–100, https://doi.org/10.1016/0273-1177(95)00079-T, 1995.

Kozlowski, T. T.: Water deficits and plant growth, Academic Press, New York, ISBN: 0124241549, https://openlibrary.org/books/OL5607338M/Water_deficits_and_plant_growth (last access: 8 February 2024), 1968.

Leasor, Z. T., Quiring, S. M., and Svoboda, M. D.: Utilizing objective drought severity thresholds to improve drought monitoring, J. Appl. Meteorol. Climatol., 59, 1455–1470, https://doi.org/10.1175/JAMC-D-19-0217.1, 2020.

Li, X., Piao, S., Huntingford, C., Peñuelas, J., Yang, H., Xu, H., Chen, A., Friedlingstein, P., Keenan, T. F., Sitch, S., Wang, X., Zscheischler, J., and Mahecha, M. D.: Global variations in critical drought thresholds that impact vegetation, Natl. Sci. Rev., 10, nwad049, https://doi.org/10.1093/nsr/nwad049, 2023.

Linés, C. and Werner, M.: How useful are seasonal forecasts for farmers facing drought? A user-based modelling approach, Clim. Serv., 39, 100595, https://doi.org/10.1016/j.cliser.2025.100595, 2025.

Linés, C., Iglesias, A., Garrote, L., Sotés, V., and Werner, M.: Do users benefit from additional information in support of operational drought management decisions in the Ebro basin?, Hydrol. Earth Syst. Sci., 22, 5901–5917, https://doi.org/10.5194/hess-22-5901-2018, 2018.

Lopez, A. and Haines, S.: Exploring the usability of probabilistic weather forecasts for water resources decision-making in the United Kingdom, Weather Clim. Soc., 9, 701–715, https://doi.org/10.1175/WCAS-D-16-0072.1, 2017.

Lovino, M. A., Pierrestegui, M. J., Müller, O. V., Müller, G. V., and Berbery, E. H.: The prevalent life cycle of agricultural flash droughts, npj Clim. Atmos. Sci., 7, 1–11, https://doi.org/10.1038/s41612-024-00618-0, 2024.

Ma, W., Zhang, X., Zhen, Q., and Zhang, Y.: Effect of soil texture on water infiltration in semiarid reclaimed land, Water Qual. Res. J., 51, 33–41, https://doi.org/10.2166/wqrjc.2015.025, 2015.

Marzban, C.: The ROC curve and the area under it as performance measures, Weather Forecast., 19, 1106–1114, https://doi.org/10.1175/825.1, 2004.

McEwen, L., Bryan, K., Black, A., Blake, J., and Afzal, M.: Science-narrative explorations of drought thresholds in the maritime Eden catchment, Scotland: implications for local drought risk management, Front. Environ. Sci., 9, 589980, https://doi.org/10.3389/fenvs.2021.589980, 2021.

Nan, Y., Chai, K. M., Lee, W. S., and Chieu, H. L.: Optimizing F-measure: a tale of two approaches, Proc. 29th Int. Conf. Mach. Learn., arXiv:1206.4625, https://doi.org/10.48550/arXiv.1206.4625, 2012.

Nguyen, N. M. and Choi, M.: Delving into flash droughts in Vietnam during last two decades using the standardized evaporative stress ratio, J. Hydrol., 634, 130669, https://doi.org/10.1016/j.jhydrol.2024.130669, 2024.

Noguera, I., Vicente-Serrano, S. M., and Domínguez-Castro, F.: The rise of atmospheric evaporative demand is increasing flash droughts in Spain during the warm season, Geophys. Res. Lett., 49, e2021GL097703, https://doi.org/10.1029/2021GL097703, 2022.

Or, D. and Lehmann, P.: Surface evaporative capacitance: how soil type and rainfall characteristics affect global-scale surface evaporation, Water Resour. Res., 55, 519–539, https://doi.org/10.1029/2018WR024050, 2019.

Otkin, J. A., Svoboda, M., Hunt, E. D., Ford, T. W., Anderson, M. C., Hain, C., and Basara, J. B.: Flash Droughts: A Review and Assessment of the Challenges Imposed by Rapid-Onset Droughts in the United States, B. Am. Meteorol. Soc., 99, 911–919, https://doi.org/10.1175/BAMS-D-17-0149.1, 2018.

Otkin, J. A., Svoboda, M., Hunt, E. D., Ford, T. W., Anderson, M. C., Hain, C., and Basara, J. B.: Flash droughts: a review and assessment of the challenges imposed by rapid-onset droughts in the United States, Bull. Am. Meteorol. Soc., 99, 911–919, https://doi.org/10.1175/BAMS-D-21-0288.1, 2022.

Padiyedath Gopalan, S., Kawamura, A., Amaguchi, H., Takasaki, T., and Azhikodan, G.: A bootstrap approach for the parameter uncertainty of an urban-specific rainfall–runoff model, J. Hydrol., 579, 124195, https://doi.org/10.1016/j.jhydrol.2019.124195, 2019.

Portele, T. C., Lorenz, C., Dibrani, B., Laux, P., Bliefernicht, J., and Kunstmann, H.: Seasonal forecasts offer economic benefit for hydrological decision making in semi-arid regions, Sci. Rep., 11, 10581, https://doi.org/10.1038/s41598-021-89564-y, 2021.

Quichimbo, E. A., Singer, M. B., Michaelides, K., Hobley, D. E. J., Rosolem, R., and Cuthbert, M. O.: DRYP 1.0: a parsimonious hydrological model of DRYland Partitioning of the water balance, Geosci. Model Dev., 14, 6893–6917, https://doi.org/10.5194/gmd-14-6893-2021, 2021.

Rojas, O.: Agricultural extreme drought assessment at global level using the FAO-Agricultural Stress Index System (ASIS), Weather Clim. Extremes, 27, 100184, https://doi.org/10.1016/j.wace.2018.09.001, 2020.

Rojas, O., Rodriguez de España, M. V., and Hernández, T.: New canicula index to study its impact on agriculture in the Central American Dry Corridor and its connection with El Niño, FAO, Rome, Italy, 67 pp., https://doi.org/10.4060/cb1818es, 2020.

Running, S., Mu, Q., Zhao, M., and Moreno, A.: MODIS/Aqua Net Evapotranspiration Gap-Filled 8-Day L4 Global 500m SIN Grid V061, NASA Land Processes Distributed Active Archive Center [data set], https://doi.org/10.5067/MODIS/MYD16A2GF.061, 2021.

Salinas Marcenaro, I., Jarquin Diaz, J. R., Ortega Flores, G. J., and Téllez Reyes, A. L.: La evapotranspiración potencial en Nicaragua usando sensores remotos, Universidad Nacional Agraria, Managua, Nicaragua, 2023, https://repositorio.una.edu.ni/4715/1/RENP40U58.pdf (last access: 8 November 2025), 2023.

Salmoral, G., Rey, D., Rudd, A., de Margon, P., and Holman, I.: A probabilistic risk assessment of the national economic impacts of regulatory drought management on irrigated agriculture, Earths Future, 7, 178–196, https://doi.org/10.1029/2018EF001092, 2019.

Sawilowsky, S.: Misconceptions leading to choosing the t test over the Wilcoxon Mann-Whitney test for shift in loca-

tion parameter, J. Mod. Appl. Stat. Methods, 4, 598–600, https://doi.org/10.22237/jmasm/1130804700, 2005.

Shyrokaya, A., Pappenberger, F., Pechlivanidis, I., Messori, G., Khatami, S., Mazzoleni, M., and Di Baldassarre, G.: Advances and gaps in the science and practice of impact-based forecasting of droughts, WIREs Water, 11, e1698, https://doi.org/10.1002/wat2.1698, 2024.

Solh, M. and van Ginkel, M.: Drought preparedness and drought mitigation in the developing world's drylands, Weather Clim. Extremes, 3, 62–66, https://doi.org/10.1016/j.wace.2014.03.003, 2014.

Soltani, A., Meinke, H., and de Voil, P.: Assessing linear interpolation to generate daily radiation and temperature data for use in crop simulations, Eur. J. Agron., 21, 133–148, https://doi.org/10.1016/S1161-0301(03)00044-3, 2004.

Son, N.-T., Chen, C.-F., Chen, C.-R., Castellón, A., Masferrer, M.-G.-M., and Recinos, L.-E.-M.: Satellite characterization of drought over cultivated areas in Central America, Int. J. Remote Sens., 39, 8505–8526, https://doi.org/10.1080/01431161.2018.1488287, 2018.

Suliman, M., Scaini, A., Manzoni, S., and Vico, G.: Soil properties modulate actual evapotranspiration, and precipitation impacts on crop yields in the USA, Sci. Total Environ., 949, 175172, https://doi.org/10.1016/j.scitotenv.2024.175172, 2024.

Sun, X., Wilcox, B. P., and Zou, C. B.: Evapotranspiration partitioning in dryland ecosystems: a global meta-analysis of in situ studies, J. Hydrol., 576, 123–136, https://doi.org/10.1016/j.jhydrol.2019.06.022, 2019.

Svoboda, M., LeComte, D., Hayes, M., Heim, R., Gleason, K., Angel, J. J. R. J., Rippey, B., Tinker, R., Palecki, M., Stooksbury, D., Miskus, D., and Stephens, D.: The Drought Monitor, Bull. Am. Meteorol. Soc., 83, 1181–1190, https://doi.org/10.1175/1520-0477(2002)083<1181:TDM>2.3.CO;2, 2002.

Takáts, E. A.: theory of crying wolf: the economics of money laundering enforcement, IMF Work. Pap., 2007, https://doi.org/10.5089/9781451866452.001.A001, 2007.

Teleubay, Z., Quiring, S. M., and Leasor, Z.: Estimation of impacts-based drought thresholds for the U.S. Corn Belt, Agr. Forest Meteorol., 372, 110715, https://doi.org/10.1016/j.agrformet.2025.110715, 2025.

Teluguntla, P., Thenkabail, P., Oliphant, A., Gumma, M., Aneece, I., Foley, D., and McCormick, R.: Landsat-Derived Global Rainfed and Irrigated-Cropland Product 30 m V001, NASA Land Processes Distributed Active Archive Center [data set], https://doi.org/10.5067/COMMUNITY/LGRIP/LGRIP30.001, 2023.

Teoh, K. K., Ibrahim, H., and Bejo, S. K.: Investigation on several basic interpolation methods for use in remote sensing application, in: 2008 IEEE Conference on Innovative Technologies in Intelligent Systems and Industrial Applications, 60–65, https://doi.org/10.1109/CITISIA.2008.4607336, 2008.

Torelló-Sentelles, H. and Franzke, C. L. E.: Drought impact links to meteorological drought indicators and predictability in Spain, Hydrol. Earth Syst. Sci., 26, 1821–1844, https://doi.org/10.5194/hess-26-1821-2022, 2022.

Tu, Z. and Yang, Y.: On the estimation of potential evaporation under wet and dry conditions, Water Resour. Res., 58, e2021WR031486, https://doi.org/10.1029/2021WR031486, 2022.

Ubeda Trujillo, I. and Rocha, L.: Dinámica de coberturas de la tierra en la subcuenca III de la cuenca sur del Lago de Managua, Nicaragua, Rev. Torreón Univ., 9, 110–128, https://doi.org/10.5377/torreon.v9i25.9857, 2020.

van der Zee Arias, A., van der Zee, J., Meyrat, A., Poveda, C., and Picado, L.: Estudio de caracterización del Corredor Seco Centroamericano. FAO, Tegucigalpa, Honduras, https://bibliotecasemiaridos.ufv.br/jspui/handle/123456789/367 (last access: 8 November 2022), 2012.

Verbist, K., Maureira, H., and Aroche, R.: Midsummer drought atlas for Central America and the Caribbean. Water Centre for Arid and Semi-arid Zones of Latin America and the Caribbean (UNESCO), 46 pp., ISBN 978-92-3-100455-1, https://unesdoc.unesco.org/ark:/48223/pf0000377790 (last access: 21 September 2023), 2018.

Walker, D. W., Oliveira, J. L., Cavalcante, L., Kchouk, S., Ribeiro Neto, G., Melsen, L. A., Fernandes, F. B. P., Mitroi, V., Gondim, R. S., Martins, E. S. P. R., and van Oel, P. R.: It's not all about drought: What "drought impacts" monitoring can reveal, Int. J. Disaster Risk Reduct., 103, 104338, https://doi.org/10.1016/j.ijdrr.2024.104338, 2024.

Wankmüller, F. J. P., Delval, L., Lehmann, P., Baur, M. J., Cecere, A., Wolf, S., Or, D., Javaux, M., and Carminati, A.: Global influence of soil texture on ecosystem water limitation, Nature, 635, 631–636, https://doi.org/10.1038/s41586-024-08089-2, 2024.

Yu, M., Zhang, J., Wei, L., Wang, G., Dong, W., and Liu, X.: Impact of soil textures on agricultural drought evolution and field capacity estimation in humid regions, J. Hydrol., 626, 130257, https://doi.org/10.1016/j.jhydrol.2023.130257, 2023.

Yuan, X., Wang, L., Wu, P., Ji, P., Sheffield, J., and Zhang, M.: Anthropogenic shift towards higher risk of flash drought over China, Nat. Commun., 10, 4661, https://doi.org/10.1038/s41467-019-12692-7, 2019.

Yuan, X., Wang, Y., Ji, P., Wu, P., Sheffield, J., and Otkin, J. A.: A global transition to flash droughts under climate change, Science, 380, 187–191, https://doi.org/10.1126/science.abn6301, 2023.

Zhu, Y., Toth, Z., Wobus, R., Richardson, D., and Mylne, K.: Economic value of ensemble-based weather forecasts, Bull. Am. Meteorol. Soc., 83, 73–83, https://doi.org/10.1175/1520-0477(2002)083<0073:TEVOEB>2.3.CO;2, 2002.